On the slowdown mechanism of water dynamics around small amphiphiles

Homsi Brandeburgo, W.; Thijmen van der Post, S.; Meijer, E.J.; Ensing, B.

DOI
10.1039/c5cp03486h

Publication date
2015

Document Version
Final published version

Published in
Physical Chemistry Chemical Physics

PCCP

PAPER

View Article Online
View Journal | View Issue

Cite this: *Phys. Chem. Chem. Phys.*, 2015, **17**, 24968

On the slowdown mechanism of water dynamics around small amphiphiles†

Wagner Homsi Brandeburgo,[ab] Sietse Thijmen van der Post,[c] Evert Jan Meijer[ab] and Bernd Ensing*[ab]

Received 16th June 2015,
Accepted 24th August 2015

DOI: 10.1039/c5cp03486h

www.rsc.org/pccp

Aqueous solvation of small amphiphilic molecules exhibits a unique and complex dynamics, that is only partially understood. A recent series of studies on the hydration of small organic compounds, such as tetramethylurea (TMU), trimethylamine *N*-oxide (TMAO) and urea, has provided strong evidence of a slowdown of the dynamics of the hydrating water molecules. However, the mechanism of this slowdown is still a matter of debate. We analyze the slowdown mechanism by combining molecular dynamics (MD) simulations, using *ab initio* and classical force field methods, with mid-infrared pump–probe spectroscopy. Aqueous solutions of TMU and of urea were studied at a 0.1 solute/solvent ratio, where we decompose the contribution of different solvating groups to the orientational dynamics. Our results reveal that two competing processes govern the H-bond breaking mechanism: H-bond switching through an associative partner exchange and a dissociative breaking characterized by an unbound state. H-bond switches are shown to occur less often near hydrophobic groups, thus creating a subset of OH groups that do not switch and therefore do not significantly reorient within the lifetime of one H-bond, but will require at least a second H-bond to be formed and broken before it may switch. Our results shed new light on the role of hydrophobic solvation in the water orientational dynamics and help to conciliate the controversy regarding the timescale separation, providing a mechanistic explanation for the observed slow component.

1 Introduction

Understanding the dynamics of aqueous solvation has proven to be a long-standing challenge. A good description of the behavior of solvating water molecules is fundamental for understanding processes in complex aqueous systems. Recent studies have addressed various aspects: the crowding effect in biological systems[1] and in nanoporous materials;[2,3] environmental effects on proton transfer;[4] the role of water in protein folding;[5] and also, in a broader context, the effect of different solute groups on the solvating water dynamics.[6–8] These studies portray the water molecules as playing a more active role in dynamical processes than a simple constituent of the solvating media.

Water dynamics has recently become the renewed subject of various interesting studies, which have raised a number of fundamental questions as well as proposals for new descriptive models. Whereas some studies further consolidate the traditional models, others demonstrate their limitations. For example, the conventional picture of liquid water with a tetrahedral structure has been challenged by the evidence of a highly asymmetric ordering, as seen from X-ray absorption.[9,10] Employing an energy decomposition method for *ab initio* MD[11,12] (AIMD) simulations, this was argued to be an asymmetry only in the strength of the H-bonds rather than in their structure. In another example, the long-established Debye diffusive model for water reorientation has been contested by the evidence that non-diffusive angular jumps[13,14] dominate the dynamics. For this reason a jump model[15] has been revised on the basis of classical force field MD (CMD) simulations[13,14] of water, proposing that large amplitude angular jumps mediate the H-bond partner exchange.

In recent years, by virtue of the development of ultrafast time-resolved spectroscopy techniques and improved capabilities of computational approaches, a large number of studies have provided detailed insight into the orientational dynamics of water molecules in aqueous solutions on the picosecond timescale.[6,16–26] Femtosecond infrared pump–probe (fs-IR),[16,17] dielectric relaxation (DR)[18] and 2D IR[19] studies of aqueous tetramethylurea (TMU) by Bakker and co-workers showed a slowdown of this dynamics at increasing solute concentrations. The slowdown was attributed to a slow component in the water reorientation resulting in a timescale separation, interpreted as

[a] *Van't Hoff Institute for Molecular Sciences, Universiteit van Amsterdam, Science Park 904, 1098 XH Amsterdam, The Netherlands. E-mail: b.ensing@uva.nl*
[b] *Amsterdam Center for Multiscale Modeling, Science Park 904, 1098 XH Amsterdam, The Netherlands*
[c] *FOM Institute AMOLF, Science Park 104, 1098 XG Amsterdam, The Netherlands*

† Electronic supplementary information (ESI) available. See DOI: 10.1039/c5cp03486h

two distinct water motions within the mixture: a faster motion assigned to bulk-like water; and a much slower motion assigned to a fraction of the water molecules that hydrate hydrophobic groups. This picture has contributed to a more general ongoing debate on hydrophobic hydration. A different view by Laage and co-workers based on CMD simulations of amphiphiles proposes instead a moderate rotational slowdown of the hydrating water that is not only due to a single slow species but rather due to a broad distribution of slowdown factors[21] based on slower H-bond exchange. It was also noted that solute aggregation plays a major role (as shown to be the case for aqueous TMU[27]) in the water reorientation dynamics,[22] since the slowdown is limited to the fraction of water in direct contact with the solute. Furthermore, NMR relaxation measurements by Qvist and Halle[20] suggest the appearance of a slow component in the orientational relaxation, which the authors attribute to all water molecules within the solute hydration shell. Another contribution was provided by Titantah and Karttunen with Car–Parrinello AIMD[23] simulations of the hydration of a single TMU molecule. They also observed a distinctive slow timescale in the orientational dynamics, supporting the notion that a subset of water molecules within the TMU solvation shell is slowed down. However, despite the extensive studies of these amphiphilic systems, a conclusive mechanistic picture that explains whether there is a timescale separation and what is the nature of a separation in such a case is still absent.

In this work, we provide novel insight into the mechanism underlying the orientational dynamics of water molecules in aqueous solution using Born–Oppenheimer AIMD and force-field CMD simulations as well as fs-IR experiments. By partitioning the water solvent molecules depending on their vicinity to hydrophilic or hydrophobic solute groups, we can compare the dynamics of water molecules in these different micro-environments. We employ a novel analysis of the H-bond network that allows us to measure the lifetimes of the H-bonds of individual water molecules and the probability that a water molecule will reorient and switch to a new H-bond partner after breaking a H-bond. With this analysis we can explain the experimentally observed slowdown of the orientational dynamics of water molecules in aqueous solutions of amphiphilic solutes and predict in which cases this leads to an observable timescale separation.

After briefly describing the methodology of our AIMD and CMD simulations and fs-IR pump–probe experiments, we first present our results on the structure and the orientational dynamics of water in (1) pure water, (2) a TMU solution, and (3) an urea solution, to confirm the aforementioned slowdown in the latter two mixtures. Next, we apply our solvent partitioning scheme and show that the slowdown is mainly localized at the water molecules of the first coordination shell of the amphiphile, but with different slowdown factors for the molecules near the hydrophilic and hydrophobic solute groups. Thirdly, we compare the H-bond lifetimes and H-bond switching probabilities of the water molecules in these different micro-environments. We conclude with a discussion on how the observed differences lead to an improved mechanistic model of the orientational dynamics of water molecules in solution.

2 Methods

2.1 *Ab Initio* molecular dynamics

The *ab initio* molecular dynamics (AIMD) simulations were performed on the basis of density functional theory (DFT) electronic structure calculations as implemented in the CP2K package.[28] We employed the BLYP functional[29,30] augmented with Grimme's D3 dispersion corrections,[31] in order to address the well known limitations of AIMD simulations in water with respect to slow diffusion and overstructure.[32,33] According to Lin *et al.*[34] dispersion corrections to the BLYP functional have shown to consistently improve the energetics and structure for liquid water. The DFT electron density is represented by a hybrid atom-centered Gaussian and auxiliary plane wave (GPW) basis, thus allowing for a fast conversion between real and reciprocal spaces.[35] The Gaussian basis consists of a triple zeta valence doubly polarized basis set whereas the plane wave expansion was cut off at 300 Ry. For the plane wave grid we applied the nearest neighbor smoothing operator NN50,[28] which for water systems was shown to be more accurate (see also the appendix of ref. 36) than a higher cutoff. Goedecker–Teter–Hutter norm-conserving pseudopotentials[37] were used to restrict the electronic state to those of the valence electrons. A Nosé–Hoover chain thermostat with a temperature of 322 K, a chain length of 4 and a time constant of 2400 fs, was used to generate an *NVT* ensemble. In addition to the D3 correction, the temperature was set higher than ambient as it has been shown[36,38] to yield good agreements with structural and dynamical properties measured from experiments of bulk water under ambient conditions.

We have performed AIMD simulations of two systems: a TMU/water solution at a solute/solvent ratio of $w = 0.1$; and a pure water system. The pure water simulation box consisted of 64 water molecules with a density of 1.000 g cm^{-3} in a periodic cubic box with dimensions of 12.42 Å. The aqueous TMU simulation box consisted of 4 TMU and 40 water molecules in a periodic box with dimensions of 12.48 Å in accordance with an experimental density of 1.013 g cm^{-3}. Each system was first equilibrated for approximately 20 ps and then sampled for 50 ps with timesteps of 0.5 fs.

2.2 Classical molecular dynamics

The force field based classical molecular dynamics (CMD) simulations were performed using the LAMMPS package,[39] with the rigid SPC-E[40] model for water and a rigid, unified atom model force field for TMU,[41] which is known to show good agreement with experimental data of thermodynamical properties and solute aggregation.[22] For urea we have used a rigid KBFF model, which, as proposed by Weerasinghe and Smith[42] and further analyzed by Mountain and Thirumalai[43] and Carr *et al.*,[6] is a good model for describing urea–urea and water–urea interactions.

We first performed a geometry optimization of the TMU for the rigid model using the Gaussian package[44] following the same procedure as in ref. 41. Considering a two-fold symmetry[45] for the TMU we have used an initial configuration with a homogeneous

distribution of water and both chiralities of TMU for the concentration w = 0.1. We have also performed CMD simulations of an urea solution with the same concentration and of pure water. All simulations were performed with each system containing approximately 500 molecules. The systems were equilibrated in the *NPT* ensemble set to represent ambient conditions for 500 ps with a timestep of 1 fs and then sampled for 200 ps in the *NVT* ensemble. We have also employed periodic boundary conditions and the Ewald summation method for the long range electrostatic interactions.

2.3 Femtosecond infrared pump–probe spectroscopy

We have performed polarization-resolved femtosecond spectroscopy in pure water and in an aqueous solution of TMU at the w = 0.1 concentration. This experiment allows us to probe the orientational dynamics by calculating the anisotropy decay. Details about the experimental setup and methodology can be found in the ESI† and in ref. 46.

2.4 H-bond and coordination number definitions

In the simulations we considered two molecules as H-bonded when the oxygen–oxygen distance is smaller than 3.3 Å, and the donor angle, $\alpha = \angle O_D{-}H_D\cdots O_A$, is larger than 120°, which was previously shown to be an adequate geometrical description.[34,47] The coordination numbers were obtained from the CMD simulations by integrating the radial distribution functions of water oxygens, $g_{O_WO_W}(r)$, up to their first minimum.

In order to calculate the H-bond switch ratio we have included one extra dynamical condition to the H-bond definition that separates definitive H-bond breaking from transient breaking. As we expect on average a 170 fs period for the 200 cm^{-1} intermolecular stretch vibration of liquid water and a duration of 140 fs for the angular jumps,[14] we used a 200 fs buffer time for the definitive breaking. Thus, only H-bonds that remain broken for at least 200 fs continuously are considered to be broken, irrespective of whether they find a new H-bond partner during this period or not. In the case that they do find a new partner within the buffer time, we consider it to be a switch, since this time is too short for a new H-bond partner to become available through translational diffusion. Also, no angular constraint was imposed for the switch, since there is a broad angular distribution for jumps,[13] and the non-diffusive motion can be uniquely defined by a subsequent exchange of H-bond partners.

2.5 Orientational autocorrelation fit

We have fitted the OACF using a novel approach that explicitly includes the librational motion as a damped harmonic oscillator, representing coherence loss between different librational frequencies, plus an exponential decay for subpicosecond motions

$$C_2(t) = A_0\left(\cos\left(\frac{2\pi t}{\tau_{sub}}\right)\cdot e^{\frac{-t}{\tau_d}} + e^{\frac{-t}{\tau_{fast}}}\right) + (1-A_0)e^{\frac{-t}{\tau_{mid}}} \quad (1)$$

Here, τ_{sub} = 0.068 ps is the average librational period, τ_d = 0.027 ps is the characteristic time for decoherence, and τ_{fast} is an average relaxation time of subpicosecond motions including rotation of the librational axis and free OH rotations.[48] The values for the average librational period and decoherence were obtained from fitting the OACFs to eqn (1); they match for all simulated systems considered in this work.

3 Results

3.1 Structure and orientational dynamics

We have characterized the H-bond network in the TMU and urea solutions by calculating the average number of water H-bonds per water molecule, and comparing it with the coordination number obtained from the radial distribution function. Fig. 1 shows that in both aqueous solutions there is a drop in the O_W–O_W coordination in comparison to that of bulk water. However, the average number of H-bonds per water molecule has only slightly decreased, thus indicating no strong perturbation of the H-bond network structure. This finding is in good agreement with previous studies,[16,49] and can also be seen from $g_{O_WO_W}(r)$ (Fig. 2a in ref. 43), in which the peak positions due to the first and second shells are undisturbed.‡ The larger water–water coordination number in pure water relative to that of the solutions implies that in pure water each molecule has a larger amount of surrounding water that it is not H-bonded with. Consequently, these surrounding water molecules have the potential to become a H-bond partner, thus making each molecule more susceptible for H-bond exchange. This seemingly subtle difference between bulk water and the aqueous solutions has an important impact on the dynamics of the H-bond network.

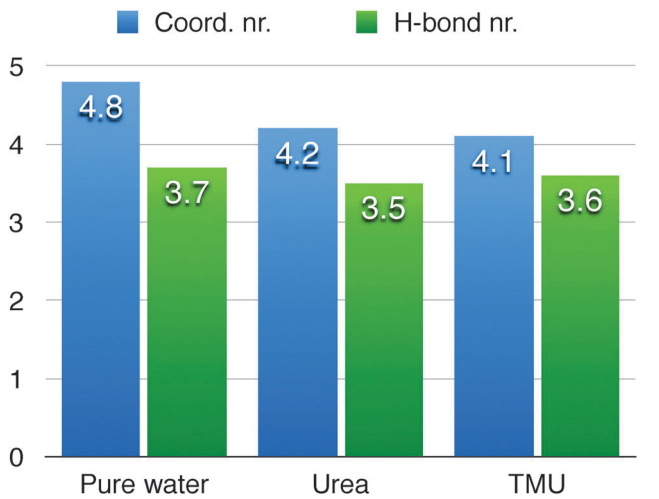

Fig. 1 Water–water coordination number and the average number of H-bond partners per molecule in pure water, TMU and urea aqueous solutions at w = 0.1 calculated with CMD.

‡ Note that the simulation boxes of pure water and both aqueous solutions contain different numbers of water molecules, and that the normalization factor of $g(r)$ does depend on these numbers. Thus, the height of the $g(r)$ peaks does not compare fairly among the different systems.

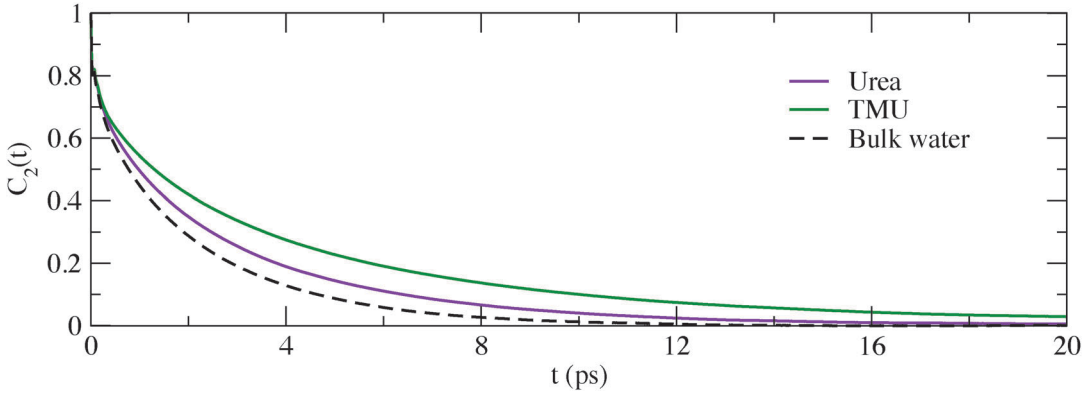

Fig. 2 A comparison between the CMD OACFs of the water molecules in pure water (black dashed line), in aqueous TMU solution (green solid line) and in aqueous urea solution (violet solid line) at w = 0.1.

In Fig. 2, we show the second rank Legendre polynomial of the calculated molecular OACF of water, for both solutions and for pure water obtained from CMD simulations

$$C_2(t) = \langle P_2[\mathbf{u}(0)\cdot\mathbf{u}(t)]\rangle \quad (2)$$

where P_2 is the Legendre polynomial, and $\mathbf{u}(t)$ the unit vector along each of the OH bonds of the water molecules. A significantly slower decay of the OACF is observed for the TMU solution in comparison to that for pure water, while the urea solution shows a notably less pronounced slowdown, in agreement with earlier work.[6] Note that the difference between the two solutions suggests a relation between the presence of hydrophobic groups and the slowdown of the water dynamics. We discuss the slowdown mechanism in more detail in the last section of this paper.

3.2 Relaxation times

Eqn (1) provides a good fit of the OACF for both the AIMD and CMD simulations of bulk water, including the initial librational bump (Fig. S1a and b in the ESI†). This second exponential characteristic time, referred to as τ_{mid}, has been assigned in the literature to large amplitude angular motions (referred to as jumps) arising from an OH group exchanging acceptor sites,[13] as its value is close to the timescale of the rate of such jumps. Eqn (1) also provides a good fit for the OACF of the urea solution, but with a larger value of τ_{mid} (Table 1). For the TMU simulations, the addition of a third exponential significantly improves the quality of the fit; whereas the fit using only two exponentials yields deviations from the data that are larger within the first picoseconds, and smaller but still consistent at longer times (Fig. S1c and d in the ESI†). This finding agrees with the simulation results of Karttunen and Titantah,[23] and with the results of the experiments by Bakker and Rezus.[16] The values obtained for the relaxation times are presented in Table 1. For experimental values and values in parentheses we fitted a mono-exponential function to the pure water OACF; and a mono-exponential function with the addition of a constant to represent a second much slower decay (or infinite relaxation time) to the TMU solution OACF in the time interval between 2 and 10 ps.

Table 1 Relaxation times obtained from fitting the OACF to eqn (1) within the indicated time interval, numbers in parentheses are from fits to a mono-exponential function in the 2–10 ps interval

System method	Fit interval (ps)	τ_{fast} (ps)	τ_{mid} (ps)	τ_{slow} (ps)
Pure water CMD	0–50			
All water		0.3	2.4 (1.9)	—
Pure water AIMD	0–15			
All water		0.5	3.1 (2.1)	—
Pure water fs-IR	2–10			
All water		—	— (2.3)	—
Urea CMD	0–12			
All water		0.6	3.6	—
Hydrophilic water		0.5	6.1	—
Hydrophobic water		0.6	5.3	—
Bulk-like water		0.3	2.7	—
TMU CMD	0–20			
All water		0.3	3.0 (2.2)	9.0 (∞)
Hydrophilic water		0.3	5.1	>20
Hydrophobic water		0.3	3.3	15.5
Bulk-like water		0.3	2.9	—
TMU AIMD	0–12			
All water		0.2	2.0 (2.8)	>12 (∞)
Hydrophilic water		0.2	3.9	>12
Hydrophobic water		0.1	2.3	>12
TMU fs-IR	2–10			
All water		—	— (2.6)	— (∞)

An extra exponential in the decay of the OACF implies the existence of an additional timescale for the orientational dynamics. Such an additional timescale has previously been interpreted as originating from slow water involved in hydrating the hydrophobic methyl groups.[16,18] On the other hand, it has also been argued in the literature that a stretched exponential model also presents a good fit for the OACF[21] of CMD simulations. This was proposed to explain the broad distribution of calculated slowdown factors; calculations which were solely based on geometrical parameters (transition state excluded volume). However, in the last section we provide evidence that the slowdown originates from a perturbation of the H-bond breaking mechanism due to the presence of hydrophobic

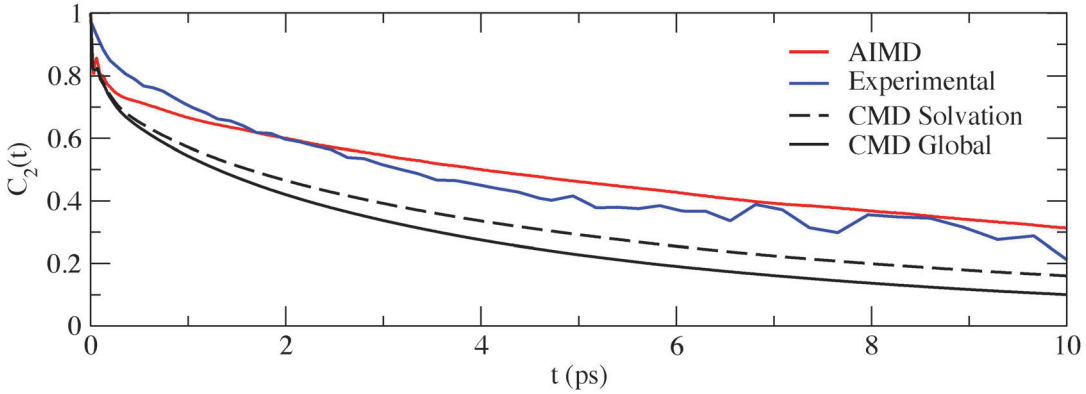

Fig. 3 Second Legendre polynomial OACF of a w = 0.1 TMU solution obtained using three different methods: AIMD (red solid line), experimental anisotropy multiplied by 5/2 (blue solid line), and CMD for all water (black solid line) and solvation water (black dashed line).

groups, thus resulting in a timescale separation in the orientational dynamics.

3.3 Experiments *versus* simulations of TMU solutions

Fig. 3 shows the experimental decay of the anisotropy (blue line) in the TMU solution in comparison with the OACFs obtained from the CMD simulation (black lines) and AIMD simulation (red line). The CMD results show a significantly faster decay of the water reorientation than the mid-infrared pump–pulse measurement, whereas the AIMD curve decays somewhat slower. The relaxation times obtained from fitting the data in the 2–10 ps interval (to exclude deviations due to *e.g.* interference between the pump and probe pulses) are shown in Table 1 in parentheses and reflect this trend. Note that for both systems – pure water and the TMU solution – the experimental and the AIMD relaxation time are very similar; with the AIMD decaying slightly faster in pure water and slightly slower in the solution, whereas the CMD results exhibit decays that are consistently faster.

A possible reason for the somewhat slower AIMD water dynamics in the TMU solution could be the absence of extended solute aggregation (as the limited AIMD unit cell contains only four solute molecules), which would decrease the amount of hydrating water and thus increase the amount of bulk-like water. Although this hypothesis cannot be tested by increasing the AIMD system due to the prohibitive cost of such a calculation, we can instead exclude the bulk-like water from the analysis of the CMD simulation. Thus, we re-compute the CMD OACF considering only water molecules that are within 4.5 Å of the methyl groups or 3.2 Å of the TMU oxygen (see the dashed line in Fig. 3). Indeed we can see that the OACF of the solvation shell water molecules exhibits a considerably slower dynamics.

We conclude that the AIMD simulation shows a OACF decay that is in good agreement with the experimental decay of the anisotropy, considering that effects due to aggregation are absent in the limited AIMD system. Instead, the quantitative results from the CMD simulations using the SPC-E force field show a faster dynamics of the water orientation. The qualitative behavior of both models is in good agreement with the experiment, as seen from the need of an extra exponential in the fit to capture the slowdown of water molecules near the TMU solute.

3.4 Partitioning the solvent water

In order to better understand the effect of different solute groups on the water dynamics, we distinguished between three types of water molecules based on their vicinity to the hydrophilic and hydrophobic solute groups. This is schematically shown in Fig. 4: (1) water close to H-bond acceptor sites of the solute (those within 3.6 Å of the solute oxygen), hereafter referred to as hydrophilic water; (2) the remainder of the hydrating water (molecules that are not hydrophilic water but

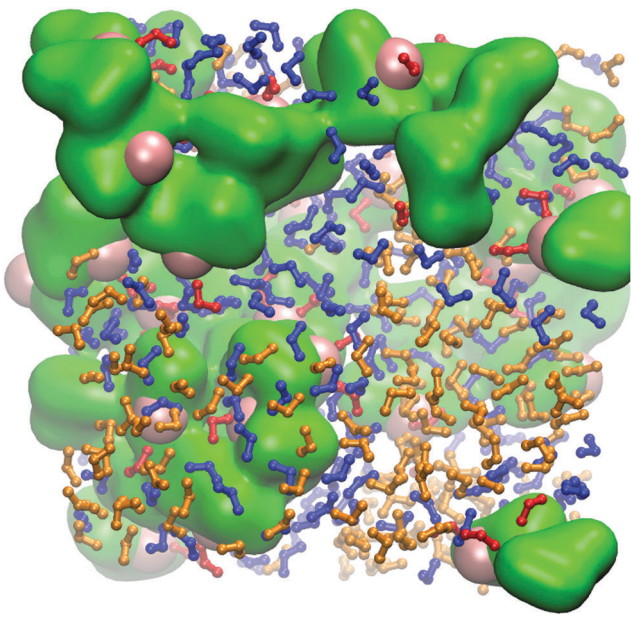

Fig. 4 A CMD snapshot of the TMU solution illustrating the different water types based on distance criteria. The TMU molecules are represented by the green and pink surfaces showing the hydrophobic and hydrophilic (oxygens) parts, respectively. Water is shown as balls and sticks, color-coded according to their location: in the vicinity of the hydrophilic side of TMU (red), close to its hydrophobic parts (blue), or bulk-like water outside the first coordination shell of TMU (orange).

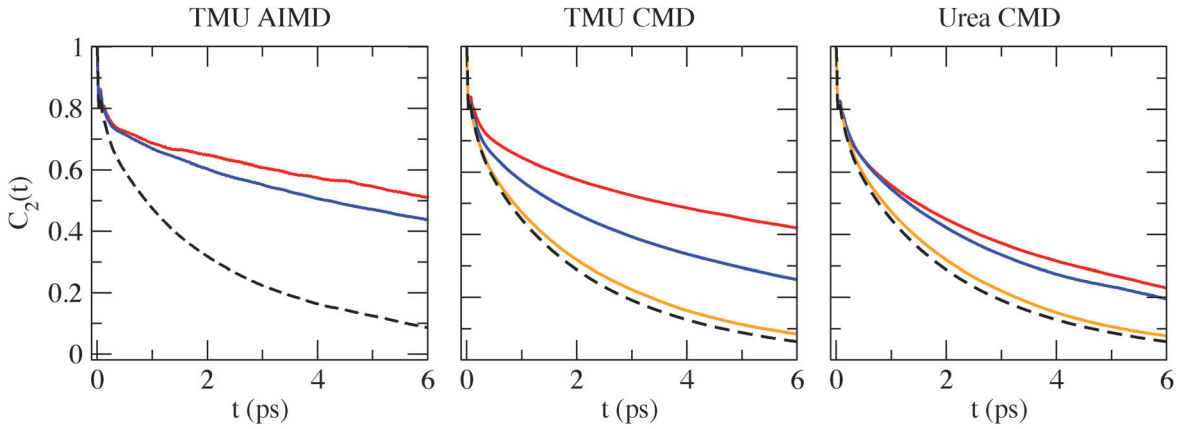

Fig. 5 Simulated OACF for the different water types from AIMD in TMU solution (a), and from CMD in TMU (b) and urea (c) solutions. The labels follow the color scheme from Fig. 4 with blue for non-hydrophilic, red for hydrophilic and orange for bulk-like water. The dashed line is from the pure water system.

still are within 4.5 Å of the methyl groups in the TMU case, and within 5.5 Å of the central carbon in the urea case), which for simplicity we refer to as hydrophobic water; and (3) the water outside the solute hydration layer, the bulk-like water. We account for water exchange between different regions by imposing a time buffer of 250 fs, after which we relabel any water molecule that has entered a new region and remained continuously in this same region according to its new position.

The OACFs computed for these three different water types in aqueous TMU and urea (see Fig. 5) clearly show that in all cases the water outside the solute hydration layer (orange lines) behaves as bulk water (black dashed lines), and that the slow-down effect of the water dynamics is largely restricted to the first solvation shell. This is consistent with the simulations by Karttunen and Titantah[23] and by Stirnemann *et al.*,[22] and with dielectric relaxation experiments.[18] Interestingly, we note that the slowdown due to the TMU is even stronger near the hydrophilic groups than near the hydrophobic groups, whereas for urea this difference is rather small. This effect seems to be exacerbated in the CMD simulations, whereas in AIMD this difference is not as pronounced.§

Could the increased slowdown of water near the hydrophilic site of TMU be caused by an enhancement of the H-bonds between these waters and the TMU carbonyl? In some cases (such as aqueous trimethylamine *N*-oxide, TMAO), a red-shift of *ca.* 100 cm^{-1} of the OH stretching band demonstrated a particularly strong H-bond between the solute and water which has been shown to cause an orientational slowdown;[50,51] however, no experimental evidence of such strengthening has been found for TMU. Moreover, this is also not observed in the water oxygen radial distribution function, as the positions of the first peak arising from the H-bond distance in TMU/water (2.75 Å) and in pure water (2.80 Å) are very similar. In order to answer this question we have calculated the vibrational spectrum of water molecules H-bonded to the TMU in the AIMD systems (see Fig. 6 – details about the calculation are found in the ESI†).

§ The OACF with error bars for the AIMD system is presented in the ESI.†

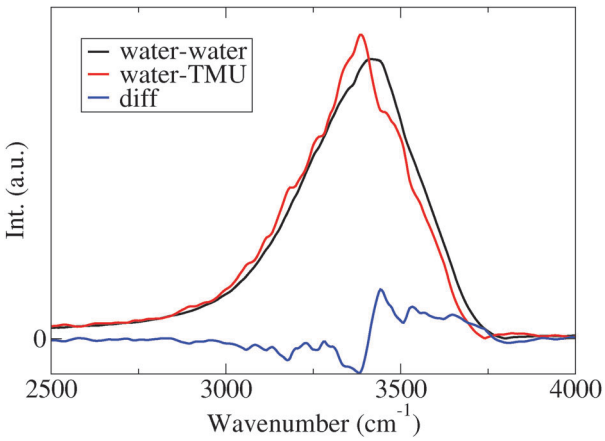

Fig. 6 Comparison of the vibrational spectrum of the hydrogens of "hydrophilic" water molecules that donate a H-bond to TMU (red) with that of hydrogens in pure water (black) from the AIMD simulations shows that the hydrogen bonds to TMU are of similar strength as those between water molecules.

The OH stretch peak does not show a significant red shift with respect to the spectrum from pure water, thus indicating similar H-bond strengths. Therefore we do not see any enhancement of these H-bonds.

3.5 Hydrogen bond dynamics

In order to quantify the mechanism of the H-bond dynamics, we distinguish between switching and non-switching H-bond breaking (as explained in the Method section). Table 2 shows the fraction of H-bond donors that switch, *i.e.* donors that break their H-bond by exchanging acceptors. The remaining fraction of broken H-bonds that do not subsequently form a new H-bond is in an unbound state (or a free OH period), after which a H-bond may be formed.¶ In this regard water

¶ In ref. 52 the authors analyze trajectories and calculate transition rates regarding the breaking of water H-bonds from a bound state to an unbound state that is similar to what is discussed in this article, however, they use different H-bond criteria.

Table 2 Average lifetime of H-bonds and the percentage of H-bonds that switch after breaking (associative breaking mechanism)

System method	$\tau_{\text{H-bond}}$ (ps)	Switches (%)
Pure water CMD		
All water	2.1	74.6
Pure water AIMD		
All water	2.2	75.9
Urea CMD		
All water	2.6	75.6
Hydrophilic water	3.1	73.8
Hydrophobic water	2.7	74.4
Bulk-like water	2.4	77.0
TMU CMD		
All water	2.9	68.8
Hydrophilic water	5.1	56.6
Hydrophobic water	3.1	65.6
Bulk-like water	2.4	74.6
TMU AIMD		
All water	4.1	62.3
Hydrophilic water	6.0	54.8
Hydrophobic water	3.9	61.2

molecules that do not switch should have a much slower reorientation time. Using the organic chemistry nomenclature to classify substitution reactions, we thus distinguish between an *associative* H-bond switching process, in which one H-bond acceptor is replaced by a new acceptor in a concerted manner by a rapid (non-diffusive) reorientation of the water molecule, and a dissociative process, in which the H-bond breaks and allows the water molecule to diffuse and eventually find in a second step a new H-bond acceptor or to reform the original H-bond.

Both the CMD and AIMD simulations show that water molecules in pure water have an average H-bond lifetime of $\tau_{\text{H-bond}}$ = 2.2 ps and 2.1 ps, respectively, after which roughly 75% perform a H-bond switch, while the remaining 25% stay uncoordinated for an average of 300 fs. The presence of TMU at the same time increases the H-bond lifetime and significantly disturbs the competition between the two H-bond breaking processes. Note, however, that the numbers for the ''bulk-like'' water in aqueous TMU are indeed very similar to those of pure water and that the increased lifetimes and lower switching propensities are seen only for water molecules in direct contact with TMU, with the largest change for the hydrophilic water molecules. In the urea case, the hydrophilic and hydrophobic water molecules also display somewhat longer H-bond lifetimes, but less substantial than in the TMU solution, and secondly, the switching propensity remains similar to that of pure water.

4 Discussion

The comparison of the average coordination of water by other water molecules in pure water, aqueous TMU and aqueous urea (Fig. 1) shows that the main difference in the solvent structure between these solutions is in the fraction of nearest neighbor waters that are not directly H-bonded. Near the solute this fraction is significantly smaller than in the bulk, thus effectively yielding a lower amount of available H-bond acceptors per water molecule. Moreover, the water orientational dynamics shows a slowdown of water in aqueous TMU and (somewhat less) in aqueous urea relative to bulk water (Fig. 2), which is predominantly restricted to the solvent water molecules in direct contact with the solutes (Fig. 5). Interestingly, the OACF for aqueous urea relaxes with a similar exponential decay as for pure water, albeit with a somewhat longer characteristic time constant, τ_{mid}, (Table 1), whereas the OACF of aqueous TMU displays an additional much slower exponential decay. The underlying mechanism for this timescale separation observed for TMU, but not for urea, can be understood from the H-bond breaking mechanism and the average H-bond lifetimes as follows.

Urea is a small polar solute that could in theory accept four H-bonds from water solvent (one at each nitrogen lone-pair, and two at the oxygen lone-pairs) and also donate four H-bonds (two by each amide group). Simulations show that in practice only the carbonyl oxygen exhibits well-defined H-bonding with the solvent, whereas the amide groups do not have a well-defined solvation structure. Mountain and Thirumalai[43] argue that the much lower number of H-bonds per urea molecule than the theoretical number of eight is due to the excluded volume of the urea molecule itself, *i.e.* a steric effect that prevents H-bonding. The urea also excludes volume from the coordination shell of nearby water molecules, which reduces the number of available H-bond acceptors around these waters. This leads to somewhat longer H-bond lifetimes (Table 2) and significantly longer τ_{mid} relaxation time constants (Table 1). Calculations performed by Skinner show that the water slowdown in urea solutions is a direct effect of the amount of surrounding ureas on individual water molecules.

The TMU case is rather different. The methyl groups are more hydrophobic, bulkier, exclude more volume and are in contact with more water molecules than the urea hydrogens. This not only leads to a further increase of the H-bond lifetimes around the TMU (see Table 2), but it even shifts the balance between associative (H-bond switching) and dissociative (unbound state formation) processes in the H-bond breaking mechanism. That is, the higher excluded volume and fewer available H-bond acceptors lead to a decreased switching propensity and favor the dissociative H-bond breaking process. It is this combined effect of the increased H-bond lifetimes and the more evenly balanced associative/dissociative competition that leads to the observed additional timescale in the orientational relaxation times of the TMU solution. The larger slowdown for the hydrophilic water compared to the hydrophobic water is therefore mainly due to the vicinity of two hydrophobic methyl groups, which form a cleavage in the hydrophilic region of the TMU thus confining the hydrating water.

To test this explanation, we have computed the H-bond survival function, $1 - \int p_{\text{SW}}(t)$, which is plotted in Fig. 7. Here, $p_{\text{SW}}(t)$ is the switch probability density calculated as the time distribution of OH switches starting from a previous switch at $t = 0$. The survival function gives the population of OH groups

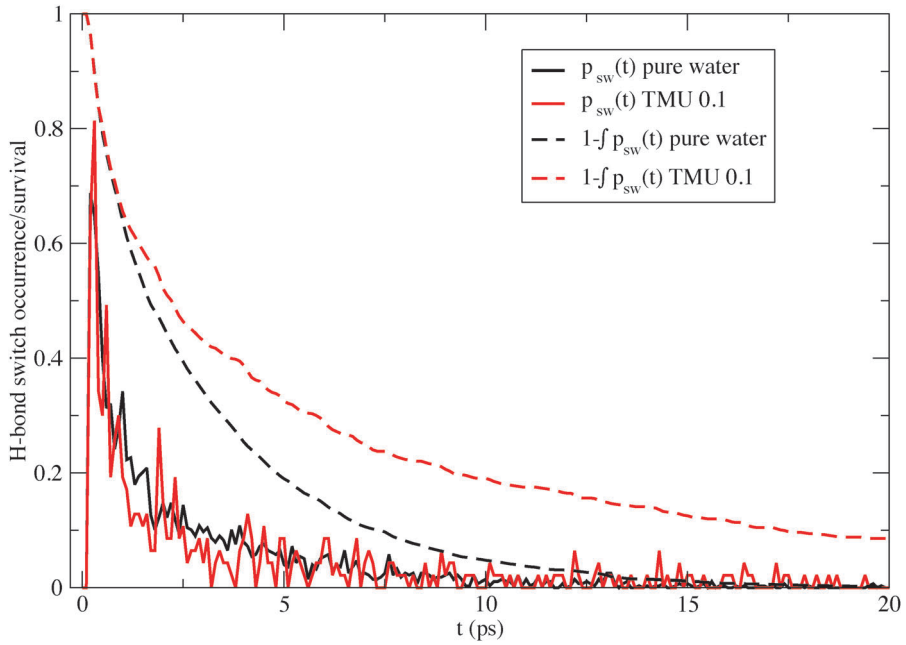

Fig. 7 H-bond switch probability density, $p_{sw}(t)$ (solid lines), and survival function, $1 - \int p_{SW}(t)$ (dashed lines), obtained from the AIMD simulations. Black lines are for pure water and red lines for the TMU solution. Results from the CMD simulations are shown in Fig. S3 of the ESI.†

that do not partake in any switch event within the time interval t. The AIMD simulation of pure water shows that less than 5% of the OH groups remain without switching within the anisotropy experimental resolution time of 10 ps. The presence of hydrophobic groups (TMU) is shown to increase this population ($\sim$20%) by adding a slowly decaying tail to this function. This extra tail has a very similar relaxation time (or decay time) τ as a slow component in the OACF (shown in ESI,† Fig. S4 and S5), thus indicating that the contribution to the OACF at longer times comes almost exclusively from switches. Moreover, the switches are not broadly distributed in time since they can only happen during an H-bond breaking event, and when one H-bond breaks *via* the dissociative process the donating OH group will have to wait at least until after a new H-bond is formed so it may break *via* switching. Depending on the dissociative H-bond breaking propensity one OH group might partake in several H-bond breaking events without switching, thus not significantly reorienting on the timescale of several H-bond lifetimes. This demonstrates how the H-bond dynamics, regarding both the H-bond lifetimes and the mechanistic switching/unbound state formation balance, is intimately connected to the observed distinct timescales of the OACF relaxation.

With this mechanistic model, we can connect the average H-bond lifetimes of the hydrophilic, hydrophobic, and bulk-like water in aqueous TMU (respectively 5.1, 3.1 and 2.4 ps as shown in Table 2) to the τ_{mid} relaxation times of the OACFs (respectively 5.1, 3.3, and 2.9 ps as seen in Table 1). For both the hydrophilic and hydrophobic water, a substantial fraction of donors breaks its H-bond *via* the dissociative mechanism (43.4% and 34.4% respectively in the CMD simulations) and, therefore, does not significantly contribute to the orientational dynamics until eventually forming a H-bond that does break *via* associative switching. This might take several H-bond lifetimes before occurring. The rather different observed τ_{slow} relaxation times (respectively $>$20 and 15.5 ps) due to the fraction of solvent waters following the dissociative mechanism reflects the different dissociative H-bond breaking propensities of 43.4% and 34.4%. Also for the urea case, the OACFs can be fitted with the three-exponential functions, which leads to somewhat slower τ_{mid} values and τ_{slow} values in the 20 ps range without significant improvement of the fit quality (see ESI†). However, due to the much lower dissociative H-bond breaking propensities (25%) no timescale separation is observed for urea.

The mechanism revealed here is rather different than the one proposed by Usui *et al.*[51] for the TMAO solution. While in the zwitter-ionic TMAO case the slowdown effect is mainly a direct consequence of a strong H-bond between water and the solute, thus causing the H-bonded water to reorient following the TMAO motion, in the TMU case this is a consequence of a confinement by the hydrophobic groups. Note that in TMU, the methyls are much closer to the hydrophilic region than in TMAO. However, we suspect that some of the slowdown that was observed within the solvation shell of the TMAO is also caused by an increase of the dissociative H-bond breaking process, it can explain the effect on water molecules close to methyl groups and water molecules more losely H-bonded to the TMAO during the H-bond breaking.

5 Conclusions

We studied the different motions that comprise the orientational dynamics of water molecules in aqueous solutions of TMU and of urea, addressing the slowdown of the dynamics of

the hydrating water molecules. *Ab initio* and classical force field molecular simulations were employed complemented by pump–probe spectroscopy measurements. We proposed an expression to fit the orientational autocorrelation function of water that explicitly takes the librational motion into account. By decomposing the orientational dynamics between different solvating regions, we were able to characterize the influence from methyl, amide and carbonyl groups on the slowdown of water reorientation. Methyl groups were shown to be the dominating factor in the slowdown of the water reorientation due to their relatively large excluded volume. In addition, we have calculated the survival function of OH groups that do not switch H-bond acceptors. We found a higher incidence of survivors around hydrophobes to be the origin of the appearance of a third relevant timescale in the orientational dynamics.

Our results suggest that the reorientation of water molecules in solution is the result of two competing processes in the H-bond breaking mechanism: a dissociative H-bond breaking process in which the OH donor finishes uncoordinated, and an associative (non-diffusive) breaking process through a concerted switching of H-bond acceptors. In the TMU solution, this competition is more evenly balanced creating a larger subset of OH groups that do not switch during a H-bond breaking and, consequently, do not significantly contribute to the water reorientation. Hence, the OH groups in this subset may only partake in a switching event at much longer times, since for that at least one new H-bond has to be formed and broken. This subset, enhanced by a significant increase in the H-bond lifetimes for water solvating hydrophobic groups, causes the appearance of a distinct slower timescale in the reorientational dynamics.

Acknowledgements

We thank Huib J. Bakker and Steven O. Nielsen for the insightful discussions. This work is part of the research program of the 'Stichting voor Fundamenteel Onderzoek der Materie (FOM)', which is financially supported by the 'Nederlandse Organisatie voor Wetenschappelijk Onderzoek (NWO)'. We acknowledge support from the Nederlandse Organisatie voor Wetenschappelijk Onderzoek (NWO) for the use of supercomputer facilities.

References

1 C. T. Andrews and A. H. Elcock, *J. Chem. Theory Comput.*, 2013, **9**, 4585–4602.
2 N. W. Ockwig, J. A. Greathouse, J. S. Durkin, R. T. Cygan, L. L. Daemen and T. M. Nenoff, *J. Am. Chem. Soc.*, 2009, **131**, 8155–8162.
3 R. Renou, A. Szymczyk and A. Ghoufi, *J. Chem. Phys.*, 2014, **140**, 044704.
4 M. Bonn, H. J. Bakker, G. Rago, F. Pouzy, J. R. Siekierzycka, A. M. Brouwer and D. Bonn, *J. Am. Chem. Soc.*, 2009, **131**, 17070–17071.
5 B. J. Bennion and V. Daggett, *Proc. Natl. Acad. Sci. U. S. A.*, 2003, **100**, 5142–5147.
6 J. K. Carr, L. E. Buchanan, J. R. Schmidt, M. T. Zanni and J. L. Skinner, *J. Phys. Chem. B*, 2013, **117**, 13291–13300.
7 P. L. Silvestrelli, *J. Phys. Chem. B*, 2009, **113**, 10728–10731.
8 T. S. van Erp and E. J. Meijer, *J. Chem. Phys.*, 2003, **118**, 8831–8840.
9 P. Wernet, D. Nordlund, U. Bergmann, M. Cavalleri, M. Odelius, H. Ogasawara, L. A. Naslund, T. K. Hirsch, L. Ojamae, P. Glatzel, L. G. M. Pettersson and A. Nilsson, *Science*, 2004, **304**, 995–999.
10 A. Nilsson and L. Pettersson, *Chem. Phys.*, 2011, **389**, 1–34.
11 T. D. Kühne and R. Z. Khaliullin, *J. Am. Chem. Soc.*, 2014, **136**, 3395–3399.
12 T. D. Kühne and R. Z. Khaliullin, *Nat. Commun.*, 2013, **4**, 1450.
13 D. Laage and J. T. Hynes, *J. Phys. Chem. B*, 2008, **112**, 14230–14242.
14 D. Laage and J. T. Hynes, *Science*, 2006, **311**, 832–835.
15 E. N. Ivanov, *JETP Lett.*, 1964, **18**, 1041–1045.
16 Y. L. A. Rezus and H. J. Bakker, *J. Phys. Chem. A*, 2008, **112**, 2355–2361.
17 Y. L. A. Rezus and H. J. Bakker, *Phys. Rev. Lett.*, 2007, **99**, 148301.
18 K.-J. Tielrooij, J. Hunger, R. Buchner, M. Bonn and H. J. Bakker, *J. Am. Chem. Soc.*, 2010, **132**, 15671–15678.
19 A. A. Bakulin, C. Liang, T. la Cour Jansen, D. A. Wiersma, H. J. Bakker and M. S. Pshenichnikov, *Acc. Chem. Res.*, 2009, **42**, 1229–1238.
20 J. Qvist and B. Halle, *J. Am. Chem. Soc.*, 2008, **130**, 10345–10353.
21 D. Laage, G. Stirnemann and J. T. Hynes, *J. Phys. Chem. B*, 2009, **113**, 2428–2435.
22 G. Stirnemann, F. Sterpone and D. Laage, *J. Phys. Chem. B*, 2011, **115**, 3254–3262.
23 J. T. Titantah and M. Karttunen, *J. Am. Chem. Soc.*, 2012, **134**, 9362–9368.
24 K. Mazur, I. A. Heisler and S. R. Meech, *J. Phys. Chem. B*, 2011, **115**, 2563–2573.
25 N. Galamba, *J. Phys. Chem. B*, 2014, **118**, 4169–4176.
26 Y. L. A. Rezus and H. J. Bakker, *Proc. Natl. Acad. Sci. U. S. A.*, 2006, **103**, 18417–18420.
27 R. Gupta and G. N. Patey, *J. Chem. Phys.*, 2014, **141**, 064502.
28 J. VandeVondele, M. Krack, F. Mohamed, M. Parrinello, T. Chassaing and J. Hutter, *Comput. Phys. Commun.*, 2005, **167**, 103–128.
29 A. D. Becke, *Phys. Rev. A: At., Mol., Opt. Phys.*, 1988, **38**, 3098–3100.
30 C. Lee, W. Yang and R. G. Parr, *Phys. Rev. B: Condens. Matter Mater. Phys.*, 1988, **37**, 785–789.
31 S. Grimme, J. Antony, S. Ehrlich and H. Krieg, *J. Chem. Phys.*, 2010, **132**, 154104.
32 J. VandeVondele, F. Mohamed, M. Krack, J. Hutter, M. Sprik and M. Parrinello, *J. Chem. Phys.*, 2005, **122**, 014515.
33 I.-F. W. Kuo, C. J. Mundy, M. J. McGrath, J. I. Siepmann, J. VandeVondele, M. Sprik, J. Hutter, B. Chen, M. L. Klein, F. Mohamed, M. Krack and M. Parrinello, *J. Phys. Chem. B*, 2004, **108**, 12990–12998.

34 I.-C. Lin, A. P. Seitsonen, I. Tavernelli and U. Rothlisberger, *J. Chem. Theory Comput.*, 2012, **8**, 3902–3910.
35 G. Lippert, J. Hutter and M. Parrinello, *Mol. Phys.*, 1997, **92**, 477–488.
36 R. Jonchiere, A. P. Seitsonen, G. Ferlat, A. M. Saitta and R. Vuilleumier, *J. Chem. Phys.*, 2011, **135**, 154503.
37 S. Goedecker, M. Teter and J. Hutter, *Phys. Rev. B: Condens. Matter Mater. Phys.*, 1996, **54**, 1703–1710.
38 S. Yoo and S. S. Xantheas, *J. Chem. Phys.*, 2011, **134**, 121105.
39 S. Plimpton, *J. Comput. Phys.*, 1995, **117**, 1–19.
40 H. J. C. Berendsen, J. R. Grigera and T. P. Straatsma, *J. Phys. Chem.*, 1987, **91**, 6269–6271.
41 P. Belletato, L. Carlos Gomide Freitas, E. P. G. Areas and P. Sergio Santos, *Phys. Chem. Chem. Phys.*, 1999, **1**, 4769–4776.
42 S. Weerasinghe and P. E. Smith, *J. Phys. Chem. B*, 2003, **107**, 3891–3898.
43 R. D. Mountain and D. Thirumalai, *J. Phys. Chem. B*, 2004, **108**, 6826–6831.
44 M. J. Frisch, G. W. Trucks, H. B. Schlegel, G. E. Scuseria, M. A. Robb, J. R. Cheeseman, G. Scalmani, V. Barone, B. Mennucci, G. A. Petersson, H. Nakatsuji, M. Caricato, X. Li, H. P. Hratchian, A. F. Izmaylov, J. Bloino, G. Zheng, J. L. Sonnenberg, M. Hada, M. Ehara, K. Toyota, R. Fukuda, J. Hasegawa, M. Ishida, T. Nakajima, Y. Honda, O. Kitao, H. Nakai, T. Vreven, J. A. Montgomery Jr., J. E. Peralta, F. Ogliaro, M. Bearpark, J. J. Heyd, E. Brothers, K. N. Kudin, V. N. Staroverov, R. Kobayashi, J. Normand, K. Raghavachari, A. Rendell, J. C. Burant, S. S. Iyengar, J. Tomasi, M. Cossi, N. Rega, M. J. Millam, M. Klene, J. E. Knox, J. B. Cross, V. Bakken, C. Adamo, J. Jaramillo, R. Gomperts, R. E. Stratmann, O. Yazyev, A. J. Austin, R. Cammi, C. Pomelli, J. W. Ochterski, R. L. Martin, K. Morokuma, V. G. Zakrzewski, G. A. Voth, P. Salvador, J. J. Dannenberg, S. Dapprich, A. D. Daniels, Ö. Farkas, J. B. Foresman, J. V. Ortiz, J. Cioslowski and D. J. Fox, *Gaussian 03, Revision C.02*, Gaussian Inc., Wallingford, CT, 2004.
45 C. S. Frampton and K. B. Parkes, *Acta Crystallogr.*, 1996, **C52**, 3246–3248.
46 S. T. van der Post and H. J. Bakker, *J. Phys. Chem. B*, 2014, **118**, 8179–8189.
47 J. P. Gotze, C. Greco, R. Mitrić, V. Bonačić-Koutecký and P. Saalfrank, *J. Comput. Chem.*, 2012, **33**, 2233–2242.
48 A. Vila Verde, P. G. Bolhuis and R. K. Campen, *J. Phys. Chem. B*, 2012, **116**, 9467–9481.
49 H. Kokubo and B. M. Pettitt, *J. Phys. Chem. B*, 2007, **111**, 5233–5242.
50 F. Sterpone, G. Stirnemann, J. T. Hynes and D. Laage, *J. Phys. Chem. B*, 2010, **114**, 2083–2089.
51 K. Usui, J. Hunger, M. Sulpizi, T. Ohto, M. Bonn and Y. Nagata, *J. Phys. Chem. B*, 2015, **119**, 10597–10606.
52 F. S. Csajka and D. Chandler, *J. Chem. Phys.*, 1998, **109**, 1125–1133.